Acta Cryst C STRUCTURAL CHEMISTRY

ISSN 2053-2296

π-Complexation and C—H hydrogen bonding in the formation of colored cocrystals

Eric Bosch,[a]* Bryce S. Moreno[b] and Nathan P. Bowling[b]

[a]Chemistry and Biochemistry Department, Missouri State University, 901 South National Avenue, Springfield, Missouri 65897, USA, and [b]Department of Chemistry, University of Wisconsin-Stevens Point, 2101 Fourth Avenue, Stevens Point, WI 54481, USA. *Correspondence e-mail: ericbosch@missouristate.edu

Received 13 January 2023
Accepted 8 March 2023

Edited by A. G. Oliver, University of Notre Dame, USA

Keywords: crystal structure; C—H···N hydrogen bond; C—H···O hydrogen bond; C—H···F hydrogen bond; π-stacking; cocrystal.

CCDC references: 2247037; 2247036

Supporting information: this article has supporting information at journals.iucr.org/c

The present study evaluates the potential combination of charge-transfer electron-donor–acceptor π–π complexation and C—H hydrogen bonding to form colored cocrystals. The crystal structures of the red 1:1 cocrystals formed from the isomeric pyridines 4- and 3-{2-[4-(dimethylamino)phenyl]ethynyl}pyridine with 1-[2-(3,5-dinitrophenyl)ethynyl]-2,3,5,6-tetrafluorobenzene, both $C_{14}H_4F_4N_2O_4{\cdot}C_{15}H_{14}N_2$, are reported. Intermolecular interaction energy calculations confirm that π-stacking interactions dominate the intermolecular interactions within each crystal structure. The close contacts revealed by Hirshfeld surface calculations are predominantly C—H interactions with N, O, and F atoms.

1. Introduction

C—H hydrogen bonding and charge-transfer (CT) π–π stacking are two of the many long-recognized intermolecular interactions within the solid state. A clear understanding of the interplay between these and other intermolecular interactions is vital for understanding the molecular arrangement of molecules within solids and the rational design of functional solid materials (Amabilino *et al.*, 2017; Kolesnichenko & Anslyn, 2017). With respect to C—H hydrogen bonding, the crystal structure of hydrogen cyanide represents the first crystallographically determined C—H···N hydrogen bond (Dulmage & Lipscomb, 1951), with a short C—H···N separation less than the sum of the van der Waals radii. The interpretation of crystallographic data that reported 'short' C—H···O separations as evidence for C—H···O hydrogen bonding in 1962 (Sutor, 1962) was followed by a brief period of controversy during the 1960s (Schwalbe, 2012). Nevertheless, C—H hydrogen bonding to O and N atoms in organic molecules soon became widely accepted (Desiraju, 1996; Steiner, 2003). Examples of C—H hydrogen bonding to O or N atoms are observed within monomolecular crystal structures, as well as secondary interactions in more complex structures. Examples with more acidic terminal alkyne C—H ($pK_a \sim 25$) include an early report of the structure of chlorobenzoylacetylene (Ferguson & Islam, 1966) and a more recent report of the structure of 4-ethynylbenzaldehyde (Dai *et al.*, 2004). Boese, however, demonstrated *sp*-C—H hydrogen bonding in the formation of cocrystals with acetylene and liquids at low temperature (Boese *et al.*, 2003). In contrast, we designed cocrystals featuring *sp*-C—H···N hydrogen bonding between solid dialkynylbenzenes and bipyridines (Bosch, 2010). Bruce and co-workers reported cocrystal formation with activated sp^2-C—H hydrogen bonding of fluorinated benzenes (Präsang *et al.*, 2013) and we exploited these more acidic fluorinated benzenes in the formation of C—H

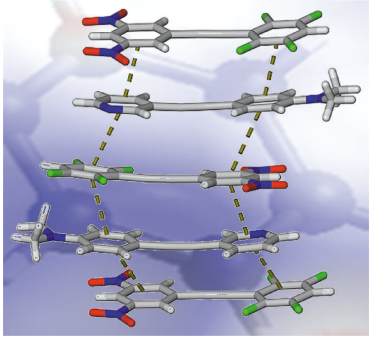

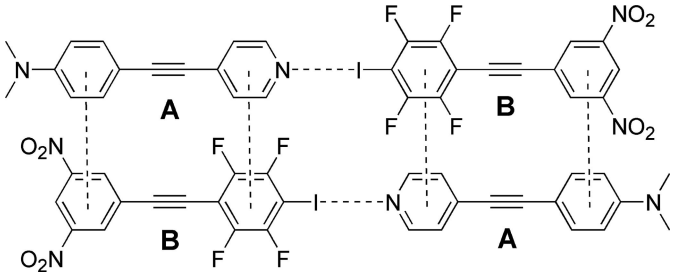

Figure 1
Previously reported co-operative halogen bonding and electron-donor–acceptor π-stacking in the 1:1 cocrystal between 1-(3,5-dinitrophenylethynyl)-2,3,5,6-tetrafluoro-4-iodobenzene and 4-[4-(dimethylamino)-phenylethynyl]pyridine.

hydrogen-bonded cocrystals with bipyridines (Bosch *et al.*, 2015).

Charge-transfer complexes, formed between an electron donor and an electron acceptor, have found application in a variety of areas, notably molecular electronics and photonics. π-Stacked charge-transfer complexes formed between an electron donor with an electron acceptor date back to the 19th century, when the quinone–hydroquinone (quinhydrone) complex was described. The crystal structure of two polymorphs of this charge-transfer complex were reported in 1958 and 1968 (Matsuda *et al.*, 1958; Sakurai, 1968). Early growth of the field is attested to by the 200-page review published in 1971 (Herbstein, 1971). Segregated stacking of donor molecules and acceptor molecules, *–D–D–D* and *–A–A–A*, is a necessity for metallic conductivity at room temperature, while semiconductor properties are common with mixed stacks of

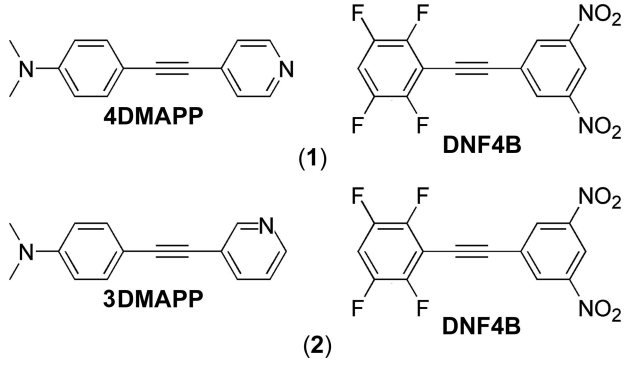

alternating donor and acceptor molecules, *–D–A–D–A–* (Goetz *et al.*, 2014). A particularly elegant example of the application of the role of colored π-stacked CT complexes in synthesis was the CT-complex-directed synthesis of rotaxanes (Basu *et al.*, 2011). We previously reported co-operative halogen bonding and CT π-stacking in the deliberate formation of colored 1:1 cocrystals (Nwachukwu *et al.*, 2018). The components in our original study were the similarly sized molecules 1-[2-(3,5-dinitrophenyl)ethynyl]-2,3,5,6-tetrafluoro-4-iodobenzene and isomeric 4-{[(dimethylamino)phenyl]-ethynyl}pyridines, as shown in Fig. 1. These components were designed so that one component was both electron-poor and a halogen-bond donor, while the second, complementary, component was electron-rich and a halogen-bond acceptor. Earlier studies had demonstrated that the electron-poor *m*-dinitrobenzene formed colored π-stacked cocrystals with electron-rich aminobenzenes (Bryce *et al.*, 1988; McNeil *et al.*, 2013). Recently, we extended this to include ditopic halogen bonding to related 4-{[(dimethylamino)phenyl]ethynyl}pyrimidines (Speetzen *et al.*, 2022).

In this article, we investigate the potential combination of C—H···N hydrogen bonding and electron-donor–acceptor π–π stacking of the similarly sized components 1-[2-(3,5-dinitrophenyl)ethynyl]-2,3,5,6-tetrafluorobenzene (**DNF4B**) with each of the isomeric pyridines 4- and 3-{2-[4-(dimethylamino)-phenyl]ethynyl}pyridine (**4DMAPP** and **3DMAPP**, respectively), and the formation of colored cocrystals (**1**) and (**2**) (see Scheme 1).

2. Experimental

2.1. Synthesis and crystallization

2.1.1. Synthesis of 1-[2-(3,5-dinitrophenyl)ethynyl]-2,3,5,6-tetrafluorobenzene (DNF4B). The product was made in a one-pot coupling–deprotection–coupling procedure from commercially available 1-bromo-2,3,5,6-tetrafluorobenzene. This bromoarene (0.500 g, 0.265 ml, 2.18 mmol) was dissolved in NEt_3 (50 ml). Argon was sparged through the solution for 20 min before $Pd(PPh_3)_2Cl_2$ (0.081 g, 0.12 mmol), CuI (0.022 g, 0.12 mmol), and ethynyltrimethylsilane (0.30 ml, 2.2 mmol) were added sequentially. This mixture was stirred at room temperature in a sealed vessel for 3 d. A separate mixture was made containing 1-iodo-3,5-dinitrobenzene (0.653 g, 2.22 mmol), $Pd(PPh_3)_2Cl_2$ (0.081 g, 0.12 mmol), and CuI (0.022 g, 0.12 mmol) dissolved in tetrahydrofuran (THF, 30 ml). Argon was sparged through this mixture for 20 min before it was transferred *via* canula into the original reaction mixture. A solution of 1 *M* tetra-*n*-butylammonium fluoride (TBAF) in THF (0.60 ml, 0.60 mmol) was introduced *via* syringe. This mixture was stirred at 323 K in a sealed vessel for 4 d. After cooling to room temperature, the mixture was transferred to a separatory funnel with CH_2Cl_2. The organic mixture was washed with water, dried with anhydrous Na_2SO_4, filtered, and concentrated. The black residue was dissolved in a minimal amount of CH_2Cl_2 and added to a flash column (silica, 7% EtOAc/93% hexane). Appropriate fractions (R_F = 0.40, EtOAc/93% hexane) were concentrated to reveal the product as a white powder (yield: 0.152 g, 0.447 mmol, 20.5%, over three steps). ^{1}H NMR (400 MHz, $CDCl_3$): δ 9.07 (*t*, *J* = 2.0 Hz, 1H), 8.73 (*d*, *J* = 2.0 Hz, 2H), 7.20 (*tt*, *J* = 9.6, 7.4 Hz, 1H). ^{13}C NMR (100 MHz, $CDCl_3$; due to limited solubility and extensive carbon–fluorine coupling, several C atoms on fluoroarene are difficult to observe): δ 148.6, 131.6, 125.3, 119.2, 108.2 (*t*, *J* = 22.6 Hz), 96.1, 79.7.

2.1.2. Preparation of cocrystals. Each of the isomeric compounds 4-, 3-, and 2-{2-[4-(dimethylamino)phenyl]ethynyl}pyridine (**4DMAPP**, **3DMAPP**, and **2DMAPP**, respec-

Table 1
Experimental details.

For both structures: $C_{14}H_4F_4N_2O_4{\cdot}C_{15}H_{14}N_2$, M_r = 562.47. Experiments were carried out at 100 K with Mo $K\alpha$ radiation. Refinement was on 372 parameters. H-atom parameters were constrained.

	(**1**)	(**2**)
Crystal data		
Crystal system, space group	Monoclinic, $P2_1/c$	Orthorhombic, *Pbcn*
a, b, c (Å)	23.8353 (8), 6.8067 (2), 16.6103 (5)	13.131 (4), 14.423 (4), 26.523 (7)
α, β, γ (°)	90, 109.104 (3), 90	90, 90, 90
V (Å^3)	2546.43 (14)	5023 (2)
Z	4	8
μ (mm^{-1})	0.12	0.12
Crystal size (mm)	0.40 × 0.20 × 0.02	0.30 × 0.20 × 0.15
Data collection		
Diffractometer	Rigaku XtaLAB Synergy Dualflex HyPix	Bruker APEXI CCD
Absorption correction	Gaussian (*CrysAlis PRO*; Rigaku OD, 2022)	Multi-scan (*SADABS*; Bruker, 2014)
T_{min}, T_{max}	0.734, 1.000	0.598, 0.746
No. of measured, independent and observed [$I > 2\sigma(I)$] reflections	50721, 6490, 4632	60342, 5554, 3976
R_{int}	0.045	0.077
(sin $\theta/\lambda)_{max}$ (Å^{-1})	0.705	0.642
Refinement		
$R[F^2 > 2\sigma(F^2)]$, $wR(F^2)$, S	0.053, 0.147, 1.02	0.056, 0.154, 1.03
No. of reflections	6490	5554
$\Delta\rho_{max}$, $\Delta\rho_{min}$ (e Å^{-3})	0.43, −0.33	0.34, −0.27

Computer programs: *CrysAlis PRO* (Rigaku OD, 2022), *SMART* (Bruker, 2014), *SAINT* (Bruker, 2014), *SHELXT2018* (Sheldrick, 2015*a*), *SHELXL2018* (Sheldrick, 2015*b*), and *X-Seed* (Barbour, 2020).

tively) were available from our previous study (Nwachukwu *et al.*, 2018). Equimolar amounts of **4DMAPP** (4.8 mg, 0.022 mmol) and **DNF4B** (7.2 mg, 0.021 mmol) were weighed into a screw cap vial. The colorless solids were dissolved in dichloromethane (2 ml) to form a clear yellow–brown solution. The vial was loosely capped and the solvent allowed to evaporate slowly, yielding a homogeneous mass of long flat rectangular plate-like red cocrystals of (**1**). Similar slow evaporation of an equimolar mixture of **DNF4B** and **3DMAPP** yielded red cocrystal (**2**). In contrast, an equimolar mixture of **DNF4B** and **2DMAPP** in a variety of solvents, including acetonitrile, acetone, chloroform, dichloromethane, nitromethane, and ethyl acetate, did not yield crystalline material, but rather a red powder was formed.

2.2. Calculations

The molecular electrostatic potential-energy surface of **DNF4B** was calculated using *Spartan'10* (Wavefunction, 2010). The geometry was optimized and the molecular electrostatic potential calculated using density functional theory (DFT) at the B3LYP/6-311++G** level with an isovalue of 0.2 electrons bohr^{-3}. The program *CrystalExplorer17* (Turner *et al.*, 2017) was used to calculate the Hirshfeld surface, as well as the intermolecular interaction energies within each crystal structure, using DFT at the B3LYP/6-311G(d,p) level. The fingerprint plots provide a breakdown of the intermolecular contacts in terms of the atoms involved along the Hirshfeld surface, including reciprocal interactions, O···H, for O or H within the defined surface. In addition to calculating the interaction energies between pairs of molecules in the crystal, *CrystalExplorer* also decomposes the interaction energy into four physically motivated terms (Mackenzie *et al.*, 2017): (i) the electrostatic energy (E_{ele}), (ii) the polarization energy (E_{pol}), (iii) the dispersion energy (E_{dis}), and (iv) the exchange–repulsion energy (E_{rep}). The breakdown of the interaction energies is collated in Tables S1–S3 (see supporting information).

2.3. X-ray structure determination

Crystal data, data collection and structure refinement details are summarized in Table 1. For each of (**1**) and (**2**), a single crystal was cut to size, immersed in viscous hydrocarbon oil, and mounted on a MiTeGen mount. All H atoms were located in difference maps, but were placed in idealized positions and refined with a riding model. Geometric parameters not routinely generated using *SHELXL* were calculated using the program *PLATON* (Spek, 2020).

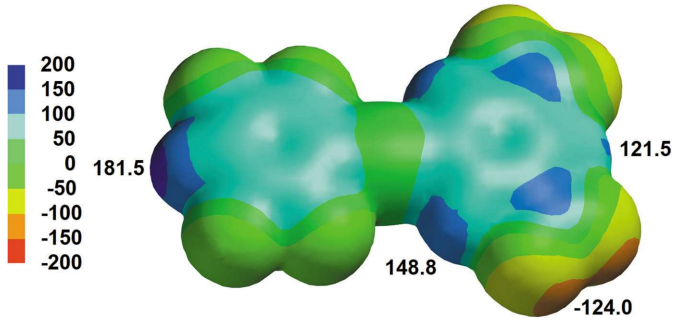

Figure 2
The molecular electrostatic potential of 1-[2-(3,5-dinitrophenyl)ethynyl]-2,3,5,6-tetrafluorobenzene (**DNF4B**) shown with all values in kJ mol^{-1}.

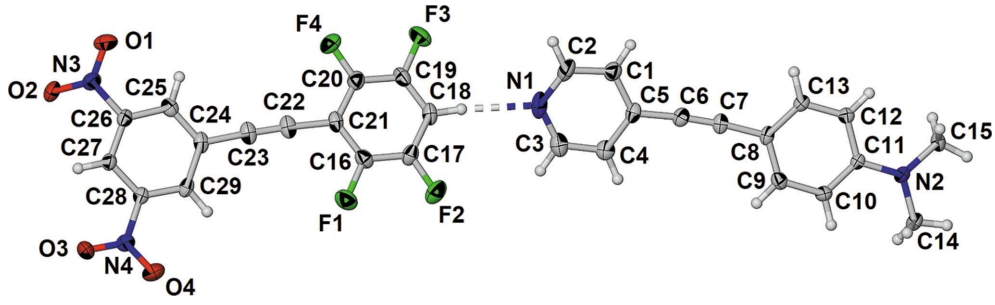

Figure 3
The molecular structure of the asymmetric unit of cocrystal (**1**), with displacement ellipsoids drawn at the 50% probability level and the C—H···N hydrogen bond shown as a dashed line.

3. Results and discussion

The compounds 4- and 3-{2-[4-(dimethylamino)phenyl] ethynyl}pyridine (**4DMAPP** and **3DMAPP**, respectively) were available from a previous study. The synthesis of 1-[2-(3,5-dinitrophenyl)ethynyl]-2,3,5,6-tetrafluorobenzene (**DNF4B**) involved a one-pot coupling–deprotection–coupling procedure. This began with the palladium-catalysed Sonogashira coupling of 1-bromo-2,3,5,6-tetrafluorobenzene with trimethylsilylacetylene. On completion of this reaction, tetrabutylammonium fluoride, to deprotect the alkyne, and 1-iodo-3,5-dinitrobenzene, to couple with the deprotected alkyne, were added to the reaction mixture. After completion of this reaction, the product **DNF4B** was isolated in modest yield. The molecular electrostatic potential of **DNF4B**, shown in Fig. 2, confirms that the proton on the tetrafluorophenyl ring has the most positive electrostatic potential at 181.5 kJ mol^{-1}, with the protons on the dinitrophenyl ring significantly less positive at 148.8 and 121.5 kJ mol^{-1}. It is noteworthy that the proton is significantly more positive than the proton in pentafluorobenzene, with an electrostatic potential of 162.5 kJ mol^{-1}. This is reasonably a consequence of the inductive effect of the two nitro groups in the second benzene ring. Also apparent is the electron-poor nature (blue color) of both arene rings.

Slow evaporation of an equimolar solution of **4DMAPP** and **DNF4B** in chloroform yielded a homogeneous mass of red crystals. X-ray analysis indicated that cocrystal (**1**) crystallized in the monoclinic space group $P2_1/c$, with one unique molecule of each component in the asymmetric unit, as shown in Fig. 3.

The aromatic rings within each molecule are almost coplanar, with dihedral angles of 10.43 (3) and 8.67 (2)° for **4DMAPP** and **DNF4B**, respectively, while the dihedral angle between the planes of the pyridyl and tetrafluorobenzene rings is 19.56 (3)°. The C—H···N hydrogen bond between the molecules has an H18···N1 separation of 2.30 Å, corresponding to 79% of the sum of the van der Waals radii (Bondi, 1964). There are also two close C—H···F contacts, with H4···F3^{i} and H10···F1^{ii} separations of 2.41 and 2.44 Å, respectively, at 92.5 and 94% of the sum of the van der Waals radii. There is one further contact that is closer than the sum of the van der Waals radii, *i.e.* a contact between a methyl proton and a nitro O atom at 96% of the sum of the van der Waals radii. The full hydrogen-bond parameters for each of these interactions are collated in Table 2. The Hirshfeld surface shows these H···N and H···F close contacts as red areas on the surface in Fig. 4.

The Hirshfeld surface fingerprint analysis of contacts to **4DMAPP** in cocrystal (**1**) provide element-to-element breakdown of the contacts (Fig. 5). The closest contact, the N···H interaction, prominent in Fig. 4, only corresponds to 5.4% of the surface area. Since this contact has the N atom within the interior of the surface, the resulting fingerprint plot is asymmetric. The F···H interactions correspond to 18.8% of the surface area, with the close contacts augmented by multiple surface–surface interactions above the sum of the van der Waals radii. The H···H contacts correspond to the highest proportion of the surface-to-surface interactions at 29.8%. As shown in the H···H fingerprint plot, there is a concentration of contacts close to the sum of the van der Waals radii at 2.4 Å. It is noteworthy that the C···C interactions are concentrated

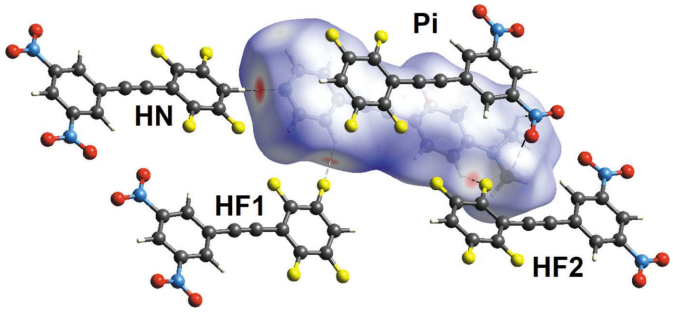

Figure 4
Hirshfeld surface for the **4DMAPP** molecule in cocrystal (**1**), with d_{norm} mapped over the surface and molecules interacting through close hydrogen contacts labeled **HN** (C—H···N) and **HF** (C—H···F), and π-stacked (**Pi**).

Table 2
Hydrogen-bond geometry (Å, °) for (**1**).

D—H···A	D—H	H···A	D···A	D—H···A
C4—H4···F3^{i}	0.95	2.41	3.207 (2)	142
C10—H10···F1^{ii}	0.95	2.44	3.193 (2)	136
C14—H14*C*···O1^{iii}	0.98	2.62	3.334 (3)	130
C18—H18···N1	0.95	2.30	3.245 (2)	173

Symmetry codes: (i) $x, -y+\frac{3}{2}, z+\frac{1}{2}$; (ii) $-x+1, -y+2, -z+2$; (iii) $-x+1, y-\frac{1}{2}, -z+\frac{3}{2}$.

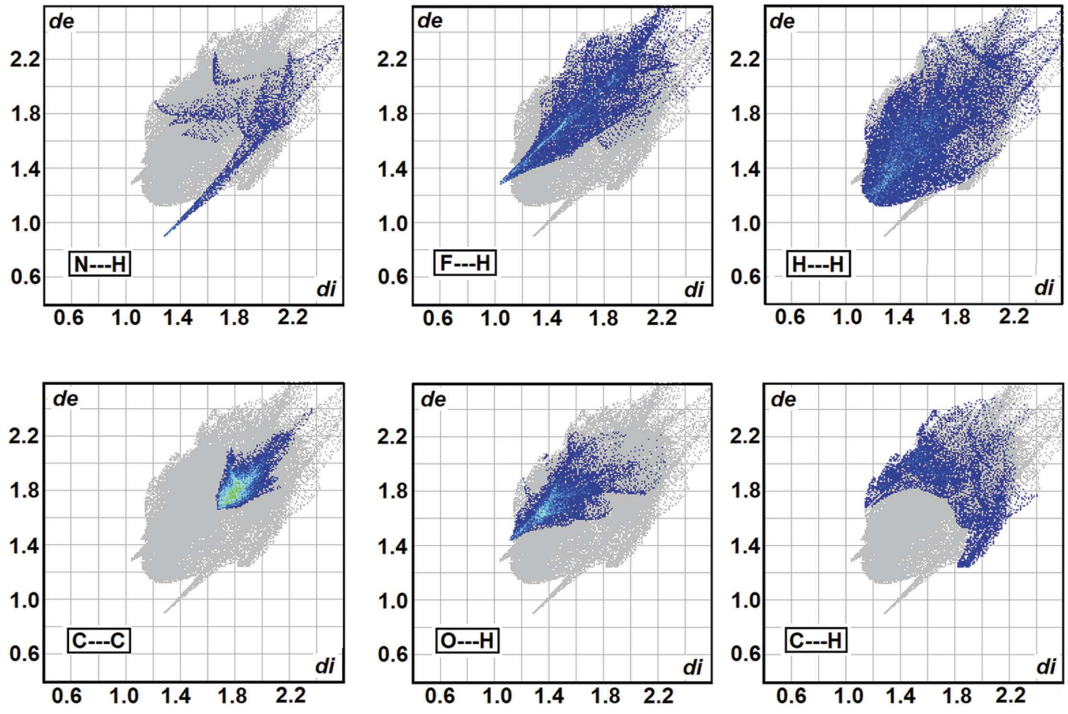

Figure 5
Fingerprint plots of contacts with the **4DMAPP** molecule in cocrystal (**1**), shown filtered by element as labeled.

near the distance of 3.6 Å commonly associated with π-stacking.

The three-dimensional structure is dominated by alternate π-stacking of **4DMAPP** and **DNF4B** molecules along the *b* axis (Fig. 6). The dinitrophenyl and 4-(dimethylamino)phenyl groups are alternately offset π-stacked, with the dimethylamino group aligned with one of the two nitro groups, with an N2···N3 separation of 3.192 (3) Å. There are two unique centroid-to-centroid distances between the two arene rings of 3.7336 (11) and 3.6825 (11) Å. Similarly, the tetrafluorophenyl and pyridyl groups are also offset π-stacked with unique centroid-to-centroid distances of 3.9685 (12) and 3.5756 (12) Å.

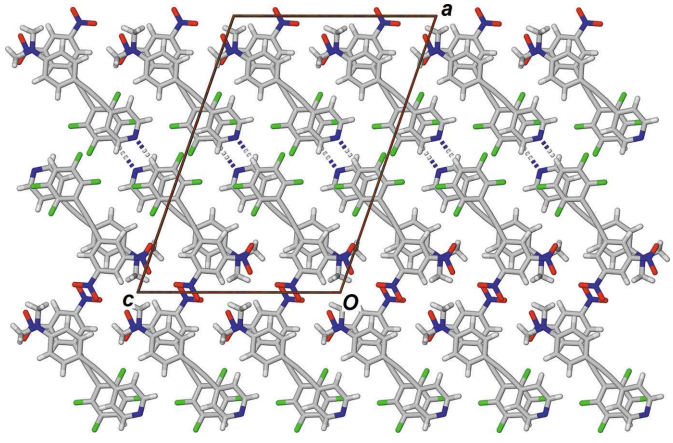

Figure 6
Partial view along the *b* axis of packing within the structure of cocrystal (**1**).

Each centroid is defined by the six atoms comprising each aromatic ring.

The intermolecular energy of interaction of **4DMAPP** with molecules closer than 3.8 Å in the structure of (**1**) was investigated using *CrystalExplorer17* (Turner *et al.*, 2017). The illustration in Fig. 7 includes only the six molecules with an energy of interaction more negative than −9 kJ mol^{-1}, for clarity of presentation. The total energy of interaction of **4DMAPP** with each of these six molecules and the associated component intermolecular electrostatic, polarization, dispersion, and repulsive energies of interaction are collated in Table 3. These data reveal that the two π-stacked molecules labeled R and O are the most cohesive, with E_{tot} = −62.5 and −60.4 kJ mol^{-1}, respectively. The major cohesive contribution to these values is from dispersion and electrostatic interactions. In both, there is a significant counteracting repulsive component. In contrast, the C—H···N hydrogen-bonded

Table 3
Intermolecular interaction energies between **4DMAPP** and molecules closer than 3.8 Å in cocrystal (**1**) (kJ mol^{-1}); colors and labels are from Fig. 7.

Color, label	E_{ele}	E_{pol}	E_{dis}	E_{rep}	E_{tot}
Red, R	−20.2	−4.3	−83.0	55.7	−62.5
Orange, O	−20.8	−4.3	−86.7	65.3	−60.4
Chartreuse, C	−18.4	−5.7	−8.5	0.0	−31.0
Blue, B	−5.6	−1.1	−22.9	18.7	−15.1
Pink, P	−4.8	−1.2	−21.2	16.1	−14.6
Turquoise, T	−3.9	−0.8	−9.9	0.0	−13.4
Green, G	−5.8	−1.5	−9.3	7.6	−10.7

Scale factors for total energy of interaction: k_{ele} = 1.057, k_{pol} = 0.740, k_{dis} = 0.871 and k_{rep} = 0.618.

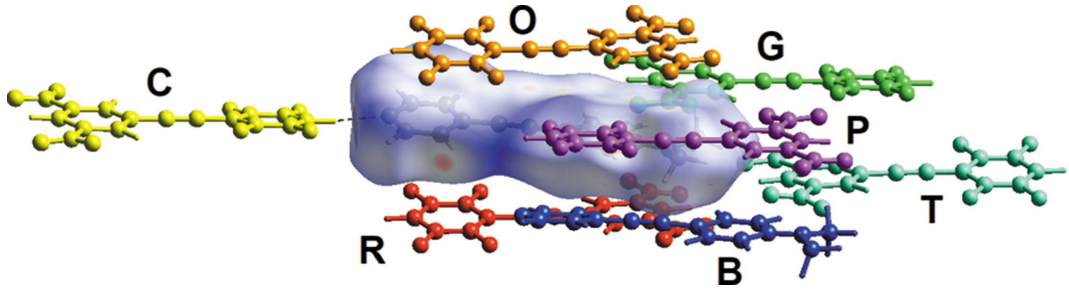

Figure 7
Color-coded **DFN4B** molecules, within 3.8 Å of a central **4DMAPP** molecule, in cocrystal (**1**) that have significant attractive intermolecular energies of interaction. Color key: R red, O orange, C chartreuse, G green, T turquoise, B blue, and P pink.

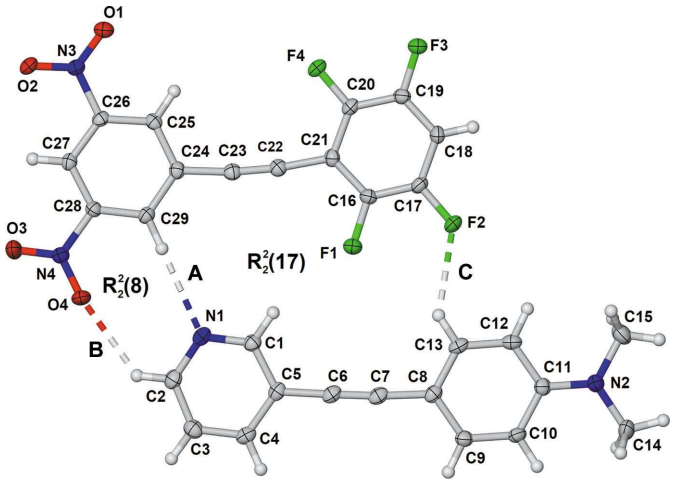

Figure 8
The molecular structure of the asymmetric unit of cocrystal (**2**), with displacement ellipsoids drawn at the 50% probability level and hydrogen bonds **A**, **B**, and **C** shown as dashed lines. The cyclic hydrogen-bonded networks are also indicated.

molecule labeled C has E_{tot} = −31.0 kJ mol^{-1}, with a major electrostatic component and modest polarization and dispersion components with a zero repulsive contribution (Table 3).

Cocrystal (**2**) also formed as a mass of red crystals on slow partial evaporation of an equimolar solution of **3DMAPP** and **DNF4B** in chloroform. Cocrystal (**2**) crystallized in the orthorhombic space group *Pbcn*, with one unique molecule of each component in the asymmetric unit, as shown in Fig. 8.

Both molecules are almost planar, with dihedral angles of 9.53 (3) and 7.26 (3)° between the aromatic rings in **3DMAPP** and **DNF4B**, respectively. In contrast to our expectation, the pyridine N1 atom forms a hydrogen bond to dinitrobenzene atom H29, rather than to the tetrafluorobenzene proton. The H29···N1 separation is 2.51 Å, *i.e.* 91% of the sum of the van der Waals radii. There is a complementary C—H···O hydrogen bond between adjacent proton H2 and nitro atom O4, resulting in a cyclic hydrogen-bonded motif, $R_2^2(8)$, indicated in Fig. 8. The third close contact between adjacent molecules is between F2 and H13, resulting in the formation of

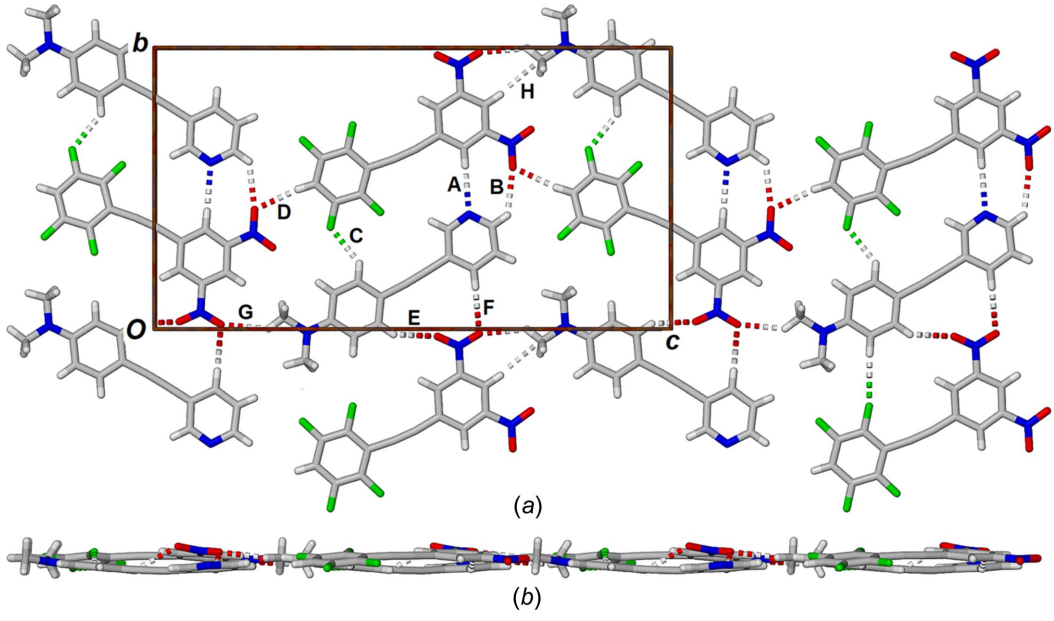

Figure 9
(*a*) Partial view of the packing in (**2**), viewed along the *a* axis, showing a single sheet of interconnected molecules. Hydrogen bonds and close contacts labeled **A**–**H** (see text) are shown as dashed lines. (*b*) Partial view of the same sheet of interconnected molecules along the *b* axis.

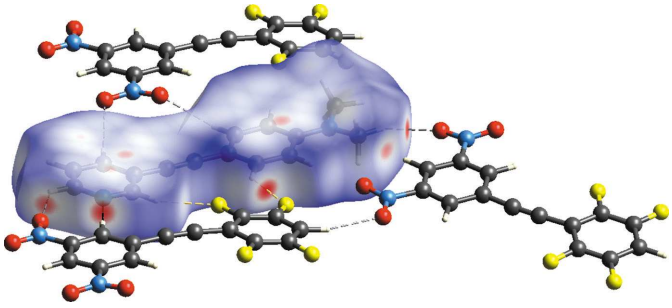

Figure 10
Hirshfeld surface for the **3DMAPP** molecule in (**2**), with d_{norm} mapped over the surface, including molecules interacting through close contacts.

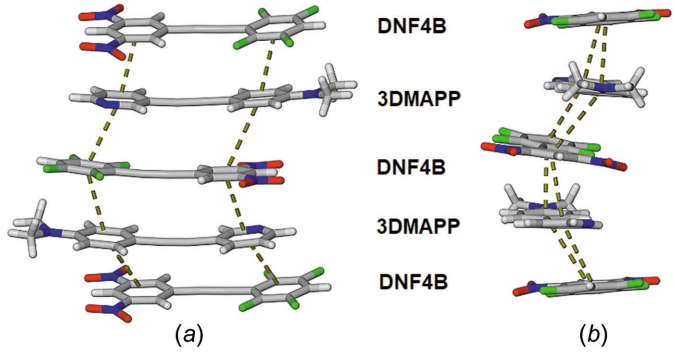

Figure 12
Two views illustrating the offset alternating π-stacking of the components within cocrystal (**2**).

a second larger cyclic hydrogen-bonded motif, $R_2^2(17)$. The separations between N1, O4, and F2, and the respective hydrogen-bonded proton are 92, 92, and 91% shorter than the respective sum of the van der Waals radii. The hydrogen bonds are labeled **A**, **B**, and **C**, respectively, in Fig. 8, and the interatomic distances and angles are collated in Table 4. Each of the components within the asymmetric unit has further C—H hydrogen-bonding interactions within the planar arrangement of molecules in the crystal (Fig. 9). Thus, the H atom on the tetrafluorophenyl ring, H18, is hydrogen bonded to atom O4^{i} (see Table 4 for symmetry codes) of a second molecule of **DNF4B**. A proton *ortho* to the alkyne group on each of the arene rings in **3DMAPP** is hydrogen bonded to a nitro O atom *via* hydrogen bonds H4$\cdots$O2^{ii} and H9$\cdots$O1^{ii}, labeled as **E** and **F** in Fig. 9. A methyl proton has a close contact to a nitro O atom (H15*C*$\cdots$O2^{iii}), with a related close contact between dinitrophenyl proton H27 and methyl-group atom C15. These close contacts, labeled **G** and **H** in Fig. 9, are 91 and 96% of the sum of the van der Waals radii, respectively. The full list of hydrogen-bond and close-contact distances and angles are given in Table 4.

The close contacts to a central **3DMAPP** molecule within (**2**) are shown in the Hirshfeld surface plot in Fig. 10, where the red areas correspond to separations between atoms less than the sum of the van der Waals radii.

The element-to-element analysis of the surface contacts within (**2**) (Fig. 11) show that O$\cdots$H and F$\cdots$H interactions dominate, with relative percentages of 22.8 and 23.6%, respectively. The fingerprint plots reveal the relative unimportance of N$\cdots$H contacts at 2.4%. The relative proportion of C$\cdots$C, C$\cdots$H, and H$\cdots$H contacts are similar at 12.0, 11.1, and 9.4%. The C$\cdots$C interactions are again concentrated near

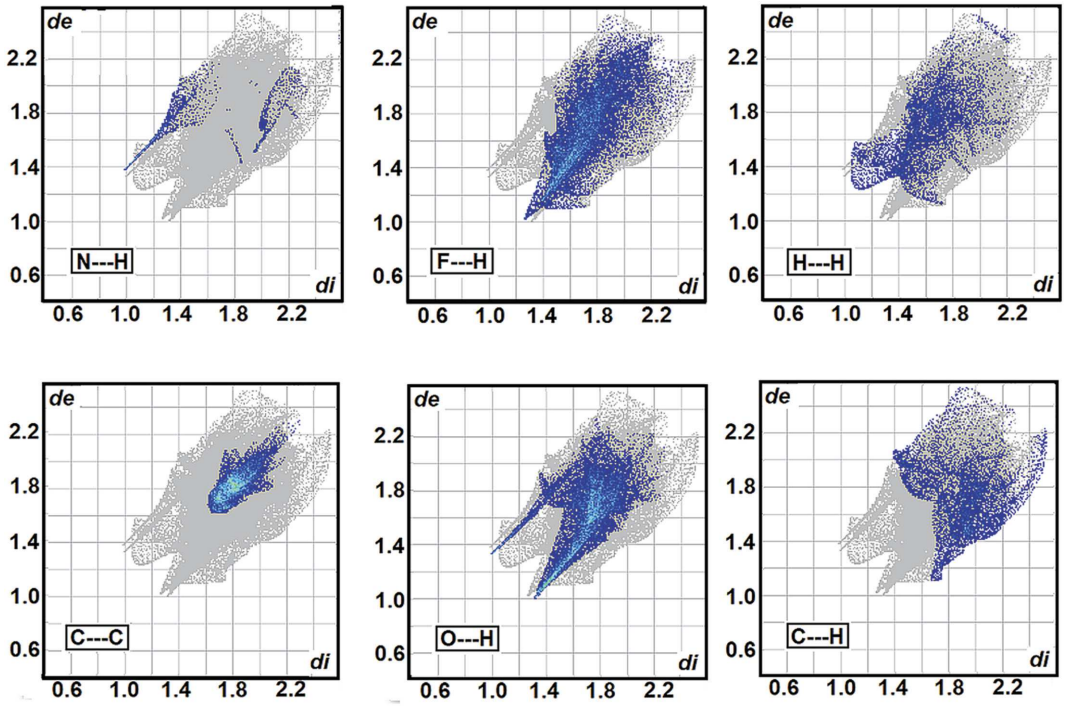

Figure 11
Fingerprint plots of contacts with the **3DMAPP** molecule in cocrystal (**2**), shown filtered by element as labeled.

Table 4
Selected hydrogen-bond and close-contact parameters (Å, °) for cocrystal (**2**).

D—H···A	Label[a]	D—H	H···A	D···A	D—H···A
C29—H29···N1	**A**	0.95	2.51	3.463 (3)	178
C2—H2···O4	**B**	0.95	2.47	3.186 (3)	132
C13—H13···F2	**C**	0.95	2.39	3.158 (3)	138
C18—H18···O4^{i}	**D**	0.95	2.46	3.398 (3)	168
C4—H4···O2^{ii}	**E**	0.95	2.46	3.398 (3)	168
C9—H9···O1^{ii}	**F**	0.95	2.59	3.319 (3)	134
C15—H15*C*···O2^{iii}	**G**	0.98	2.47	3.257 (3)	137
C27—H27···C15^{iii}	**H**	0.95	2.79	3.398 (3)	174

Note: (*a*) labels in Figs. 8 and 9. Symmetry codes: (i) $x, -y+1, z-\frac{1}{2}$; (ii) $x, y-1, z$; (iii) $x, -y+1, z-\frac{1}{2}$.

the distance of 3.6 Å commonly associated with π-stacking, as noted in cocrystal (**1**).

The molecules within cocrystal (**2**) are π-stacked along the *a* axis, with alternating **3DMAPP** and **DNF4B** molecules. The orientation of the individual donor and acceptor molecules alternates within each stack (Fig. 12).

Thus, the dinitrophenyl ring is π-stacked with the pyridyl ring [centroid–centroid distance = 3.5086 (16) Å] and offset π-stacked with the (dimethylamino)phenyl ring [centroid–centroid distance = 4.2159 (17) Å and slippage = 2.752 Å]. Similarly, the tetrafluorophenyl ring is π-stacked with the (dimethylamino)phenyl ring [centroid–centroid distance = 3.7137 (17) Å] and the pyridyl ring [centroid-centroid distance = 3.6310 (16) Å]. Intermolecular interaction energies were calculated for molecules within 3.8 Å of **3DMAPP**, and the five molecules with the most significant interaction energies are shown in Fig. 13, with the results tabulated in Table 5.

The π-stacked blue molecule (labeled B) has the most attractive interaction with **3DMAPP** (E_{tot} = −60.6 kJ mol^{-1}), with a very high dispersive contribution as a result of the most extensive π–π interaction involving the central molecule and high repulsive contribution. The offset π-stacked purple (P) molecule has somewhat lower dispersive and repulsive contributions and an E_{tot} = −53.9 kJ mol^{-1}. The chartreuse molecule (C), with three hydrogen bonds to the central **3DMAPP** molecule, has the most favorable electrostatic interaction.

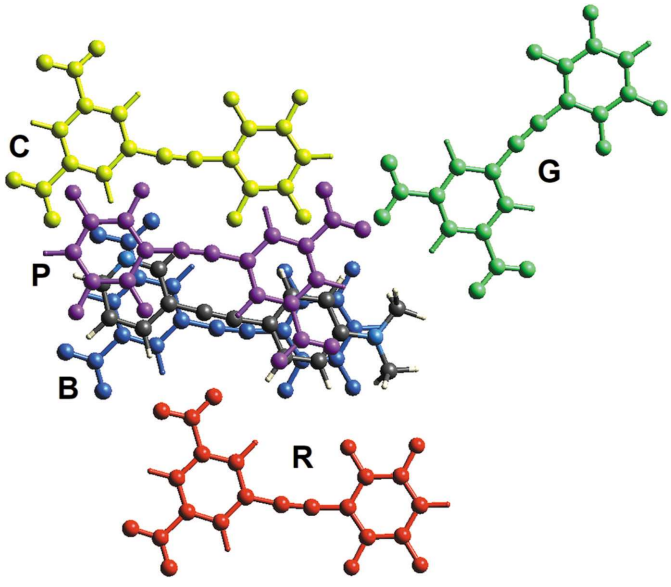

Figure 13
Color-coded molecules within 3.8 Å of the central **3DMAPP** molecule, shown in gray, in cocrystal (**2**) that have significant attractive intermolecular interaction energies. Color key: R red, G green, C chartreuse, B blue and P purple.

Table 5
Intermolecular energies of interaction of **4DMAPP** with molecules within 3.8 Å in cocrystal (**2**) in kJ mol^{-1}; colors and labels are from Fig. 13.

Color/label	E_{ele}	E_{pol}	E_{dis}	E_{rep}	E_{tot}
Blue, B	−18.9	−5.3	−92.7	71.3	−60.6
Purple, P	−19.3	−4.1	−70.0	49.5	−53.9
Chartreuse, C	−23.4	−4.5	−24.1	32.1	−29.2
Green, G	−6.6	−1.1	−13.6	0.0	−19.6
Red, R	−4.4	−1.8	−23.1	19.4	−14.1

Scale factors for total energy of interaction: k_{ele} = 1.057, k_{pol} = 0.740, k_{dis} = 0.871 and k_{rep} = 0.618.

4. Conclusions

The two red 1:1 cocrystals reported here both feature attractive π-stacking and C—H hydrogen bonding. The detailed description of each structure reveals the complexity within two closely related 1:1 cocrystals and the need for further study related to the interplay between noncovalent intermolecular interactions. Thus, while the best C—H hydrogen-bond donor, *i.e.* the proton on the tetrafluorophenyl group, and the best hydrogen-bond acceptor, *i.e.* the pyridine N atom, form a C—H···N hydrogen bond in cocrystal (**1**), they do not in cocrystal (**2**). Also, the most electron-rich arene ring, (methylamino)phenyl, and the most electron-poor arene ring, dinitrophenyl, are alternately π-stacked in cocrystal (**1**). In cocrystal (**2**), the π-stacking motif also has π-stacking interactions between the (methylamino)phenyl and the tetrafluorophenyl groups.

Acknowledgements

EB acknowledges The National Science Foundation, Division of Chemistry, Major Research Instrumentation Program, that funded the purchase of the Synergy-S X-ray diffractometer.

Funding information

Funding for this research was provided by: National Science Foundation, Directorate for Mathematical and Physical Sciences (grant No. CHE-1903593); National Science Foundation, Division of Chemistry, Major Research Instrumentation Program (award No. 2117129).

References

Amabilino, D. B., Smith, D. K. & Steed, J. W. (2017). *Chem. Soc. Rev.* **46**, 2404–2420.
Barbour, L. J. (2020). *J. Appl. Cryst.* **53**, 1141–1146.

Basu, S., Coskun, A., Friedman, D. C., Olson, M. A., Benítez, D., Tkatchouk, E., Barin, G., Yang, J., Fahrenbach, A. C., Goddard, W. A. III & Stoddart, J. F. (2011). *Chem. Eur. J.* **17**, 2107–2119.
Boese, R., Kirchner, M. T., Billups, W. E. & Norman, L. R. (2003). *Angew. Chem. Int. Ed.* **42**, 1961–1963.
Bondi, A. (1964). *J. Phys. Chem.* **68**, 441–451.
Bosch, E. (2010). *Cryst. Growth Des.* **10**, 3808–3813.
Bosch, E., Bowling, N. P. & Darko, J. (2015). *Cryst. Growth Des.* **15**, 1634–1641.
Bruker (2014). *SMART*, *SADABS*, and *SAINT*. Bruker AXS Inc., Madison, Wisconsin, USA.
Bryce, M. R. & Davies, S. R. (1988). *Synth. Met.* **25**, 25–28.
Dai, C., Yuan, Z., Collings, J. C., Fasina, T. M., Thomas, R. L., Roscoe, K. P., Stimson, L. M., Yufit, D. S., Batsanov, A. S., Howard, J. A. K. & Marder, T. B. (2004). *CrystEngComm*, **6**, 184–188.
Desiraju, G. R. (1996). *Acc. Chem. Res.* **29**, 441–449.
Dulmage, W. J. & Lipscomb, W. N. (1951). *Acta Cryst.* **4**, 330–334.
Ferguson, G. & Islam, K. M. S. (1966). *J. Chem. Soc. B*, pp. 593–600.
Goetz, K. P., Vermeulen, D., Payne, M. E., Kloc, C., McNeil, L. E. & Jurchescu, O. D. (2014). *J. Mater. Chem. C*, **2**, 3065–3076.
Herbstein, F. H. (1971). *Perspectives in Structural Chemistry* Vol. 4, edited by J. D. Dunitz & J. A. Ibers, pp. 166–395. London: Wiley.
Kolesnichenko, I. & Anslyn, E. V. (2017). *Chem. Soc. Rev.* **46**, 2385–2390.
Mackenzie, C. F., Spackman, P. R., Jayatilaka, D. & Spackman, M. A. (2017). *IUCrJ*, **4**, 575–587.
Matsuda, H., Osaki, K. & Nitta, I. (1958). *Bull. Chem. Soc. Jpn*, **31**, 611–620.
McNeil, S. K., Kelley, S. P., Beg, C., Cook, H., Rogers, R. D. & Nikles, D. E. (2013). *Appl. Mater. Interfaces*, **5**, 7647–7653.
Nwachukwu, C. I., Kehoe, Z. R., Bowling, N. P., Speetzen, E. D. & Bosch, E. (2018). *New J. Chem.* **42**, 10615–10622.
Präsang, C., McAllister, L. J., Whitwood, A. C. & Bruce, D. W. (2013). *CrystEngComm*, **15**, 8947–8958.
Rigaku OD (2022). *CrysAlis PRO*. Rigaku Oxford Diffraction, Houston, Texas, USA.
Sakurai, T. (1968). *Acta Cryst.* B**24**, 403–412.
Schwalbe, C. H. (2012). *Crystallogr. Rev.* **18**, 191–206.
Sheldrick, G. M. (2015*a*). *Acta Cryst.* A**71**, 3–8.
Sheldrick, G. M. (2015*b*). *Acta Cryst.* C**71**, 3–8.
Speetzen, E. D., Nwachukwu, C. I., Bowling, N. P. & Bosch, E. (2022). *Molecules*, **27**, 1527.
Spek, A. L. (2020). *Acta Cryst.* E**76**, 1–11.
Steiner, T. (2003). *Crystallogr. Rev.* **9**, 183–184
Sutor, D. J. (1962). *Nature*, **195**, 68–69.
Turner, M. J., McKinnon, J. J., Wolff, S. K., Gromwood, D. J., Spackman, P. R., Jayatilaka, D. & Spackman, M. A. (2017). *CrystalExplorer*. Version 17.5. University of Western Australia. https://crystalexplorer.net/.
Wavefunction (2010). *Spartan'10*. Wavefunction Inc., Irvine, CA, USA. https://www.wavefun.com/products.

supporting information

Acta Cryst. (2023). C**79**, 149-157 [https://doi.org/10.1107/S2053229623002231]

π-Complexation and C—H hydrogen bonding in the formation of colored cocrystals

Eric Bosch, Bryce S. Moreno and Nathan P. Bowling

Computing details

Data collection: *CrysAlis PRO* (Rigaku OD, 2022) for (1); *SMART* (Bruker, 2014) for (2). Cell refinement: *CrysAlis PRO* (Rigaku OD, 2022) for (1); *SMART* (Bruker, 2014) for (2). Data reduction: *CrysAlis PRO* (Rigaku OD, 2022) for (1); *SAINT* (Bruker, 2014) for (2). For both structures, program(s) used to solve structure: SHELXT2018 (Sheldrick, 2015a); program(s) used to refine structure: *SHELXL2018* (Sheldrick, 2015b); molecular graphics: *X-SEED* (Barbour, 2020); software used to prepare material for publication: *X-SEED* (Barbour, 2020).

4-{2-[4-(Dimethylamino)phenyl]ethynyl}pyridine; 1-[2-(3,5-dinitrophenyl)ethynyl]-2,3,5,6-tetrafluorobenzene (1)

Crystal data

$C_{14}H_4F_4N_2O_4 \cdot C_{15}H_{14}N_2$
$M_r = 562.47$
Monoclinic, $P2_1/c$
$a = 23.8353$ (8) Å
$b = 6.8067$ (2) Å
$c = 16.6103$ (5) Å
$\beta = 109.104$ (3)°
$V = 2546.43$ (14) Å^3
$Z = 4$
$F(000) = 1152$
$D_x = 1.467$ Mg m^{-3}
Mo $K\alpha$ radiation, $\lambda = 0.71073$ Å
Cell parameters from 4996 reflections
$\theta = 2.6$–$26.0°$
$\mu = 0.12$ mm^{-1}
$T = 100$ K
Cut block, red
0.40 × 0.20 × 0.02 mm

Data collection

Rigaku XtaLAB Synergy Dualflex HyPix diffractometer
Radiation source: micro-focus sealed X-ray tube, PhotonJet (Mo) X-ray Source
Mirror monochromator
Detector resolution: 10.0000 pixels mm^{-1}
ω scans
Absorption correction: gaussian (CrysAlis PRO; Rigaku OD, 2022)
$T_{min} = 0.734$, $T_{max} = 1.000$
50721 measured reflections
6490 independent reflections
4632 reflections with $I > 2\sigma(I)$
$R_{int} = 0.045$
$\theta_{max} = 30.1°$, $\theta_{min} = 2.5°$
$h = -32 \rightarrow 30$
$k = -8 \rightarrow 9$
$l = -21 \rightarrow 22$

Refinement

Refinement on F^2
Least-squares matrix: full
$R[F^2 > 2\sigma(F^2)] = 0.053$
$wR(F^2) = 0.147$
$S = 1.02$
6490 reflections
372 parameters
0 restraints
Hydrogen site location: inferred from neighbouring sites
H-atom parameters constrained

$w = 1/[\sigma^2(F_o^2) + (0.0582P)^2 + 1.7045P]$
where $P = (F_o^2 + 2F_c^2)/3$
$(\Delta/\sigma)_{max} < 0.001$

$\Delta\rho_{max} = 0.43$ e Å^{-3}
$\Delta\rho_{min} = -0.33$ e Å^{-3}

Special details

Geometry. All esds (except the esd in the dihedral angle between two l.s. planes) are estimated using the full covariance matrix. The cell esds are taken into account individually in the estimation of esds in distances, angles and torsion angles; correlations between esds in cell parameters are only used when they are defined by crystal symmetry. An approximate (isotropic) treatment of cell esds is used for estimating esds involving l.s. planes.

Fractional atomic coordinates and isotropic or equivalent isotropic displacement parameters (Å^2)

	x	*y*	*z*	U_{iso}*/U_{eq}
F1	0.28456 (5)	0.8952 (2)	0.56244 (9)	0.0523 (3)
O1	0.16990 (7)	0.8728 (3)	0.02012 (10)	0.0569 (4)
N1	0.56110 (8)	0.8842 (3)	0.77962 (11)	0.0479 (5)
C1	0.66347 (9)	0.9153 (3)	0.86474 (11)	0.0377 (4)
H1	0.703142	0.939993	0.866805	0.045*
F2	0.38279 (6)	0.8967 (2)	0.69917 (7)	0.0542 (3)
O2	0.07428 (7)	0.8889 (3)	−0.01819 (9)	0.0622 (5)
N2	0.87535 (7)	0.8433 (3)	1.43508 (9)	0.0374 (4)
C2	0.61747 (10)	0.9154 (3)	0.78774 (12)	0.0456 (5)
H2	0.627064	0.939357	0.737419	0.055*
F3	0.49846 (5)	0.7940 (2)	0.52233 (9)	0.0590 (4)
O3	−0.02267 (7)	0.8563 (4)	0.19380 (11)	0.0835 (8)
N3	0.12366 (8)	0.8794 (3)	0.03622 (10)	0.0446 (4)
C3	0.54875 (9)	0.8501 (3)	0.85129 (14)	0.0438 (5)
H3	0.508550	0.827434	0.847032	0.053*
F4	0.40060 (6)	0.8014 (2)	0.38489 (7)	0.0545 (3)
O4	0.02756 (8)	0.8887 (4)	0.32412 (11)	0.0803 (7)
N4	0.02398 (7)	0.8720 (3)	0.25021 (10)	0.0388 (4)
C4	0.59125 (8)	0.8459 (3)	0.93119 (12)	0.0364 (4)
H4	0.580164	0.821170	0.980224	0.044*
C5	0.65027 (8)	0.8782 (3)	0.93908 (11)	0.0302 (4)
C6	0.69531 (8)	0.8735 (3)	1.02069 (11)	0.0316 (4)
C7	0.73052 (8)	0.8709 (3)	1.09104 (11)	0.0311 (4)
C8	0.76868 (7)	0.8680 (2)	1.17791 (10)	0.0280 (3)
C9	0.74375 (8)	0.8652 (3)	1.24264 (11)	0.0319 (4)
H9	0.701761	0.866569	1.228328	0.038*
C10	0.77861 (8)	0.8605 (3)	1.32728 (11)	0.0325 (4)
H10	0.760409	0.859549	1.370321	0.039*
C11	0.84062 (7)	0.8572 (3)	1.35024 (10)	0.0270 (3)
C12	0.86623 (7)	0.8646 (2)	1.28534 (10)	0.0272 (3)
H12	0.908213	0.865951	1.299570	0.033*
C13	0.83073 (7)	0.8699 (3)	1.20077 (10)	0.0280 (3)
H13	0.848688	0.875039	1.157496	0.034*
C14	0.84830 (9)	0.8579 (3)	1.50130 (11)	0.0415 (5)
H14A	0.828751	0.985830	1.497565	0.062*
H14B	0.878988	0.844721	1.557196	0.062*

H14C	0.818879	0.753012	1.493936	0.062*
C15	0.93842 (8)	0.8670 (3)	1.45946 (12)	0.0404 (4)
H15A	0.954801	0.767690	1.430668	0.061*
H15B	0.956009	0.851147	1.521291	0.061*
H15C	0.947599	0.998385	1.443099	0.061*
C16	0.33747 (8)	0.8741 (3)	0.55145 (12)	0.0342 (4)
C17	0.38804 (9)	0.8729 (3)	0.62161 (11)	0.0351 (4)
C18	0.44282 (8)	0.8476 (3)	0.61351 (12)	0.0356 (4)
H18	0.477752	0.846873	0.661968	0.043*
C19	0.44556 (8)	0.8234 (3)	0.53314 (13)	0.0372 (4)
C20	0.39544 (8)	0.8263 (3)	0.46219 (11)	0.0354 (4)
C21	0.33970 (7)	0.8529 (3)	0.46970 (11)	0.0313 (4)
C22	0.28676 (8)	0.8556 (3)	0.39792 (12)	0.0363 (4)
C23	0.24107 (8)	0.8576 (3)	0.34014 (12)	0.0368 (4)
C24	0.18501 (8)	0.8612 (3)	0.27323 (11)	0.0313 (4)
C25	0.18202 (8)	0.8654 (3)	0.18809 (12)	0.0328 (4)
H25	0.217176	0.862299	0.173019	0.039*
C26	0.12667 (8)	0.8741 (3)	0.12585 (11)	0.0325 (4)
C27	0.07436 (8)	0.8779 (3)	0.14376 (10)	0.0307 (4)
H27	0.036964	0.885664	0.099941	0.037*
C28	0.07892 (7)	0.8700 (3)	0.22857 (11)	0.0292 (3)
C29	0.13262 (8)	0.8613 (3)	0.29382 (11)	0.0316 (4)
H29	0.133930	0.855430	0.351555	0.038*

Atomic displacement parameters (Å²)

	U^{11}	U^{22}	U^{33}	U^{12}	U^{13}	U^{23}
F1	0.0337 (6)	0.0577 (8)	0.0685 (8)	0.0075 (6)	0.0209 (6)	−0.0085 (6)
O1	0.0573 (10)	0.0682 (11)	0.0561 (9)	0.0014 (8)	0.0333 (8)	0.0001 (8)
N1	0.0459 (10)	0.0446 (10)	0.0386 (9)	0.0085 (8)	−0.0062 (7)	−0.0064 (8)
C1	0.0350 (9)	0.0434 (11)	0.0330 (9)	0.0064 (8)	0.0088 (7)	0.0028 (8)
F2	0.0701 (9)	0.0547 (8)	0.0378 (6)	0.0059 (7)	0.0175 (6)	−0.0106 (6)
O2	0.0533 (9)	0.0982 (15)	0.0290 (7)	−0.0181 (9)	0.0053 (7)	−0.0041 (8)
N2	0.0308 (8)	0.0565 (11)	0.0235 (7)	0.0034 (7)	0.0071 (6)	0.0009 (7)
C2	0.0516 (12)	0.0526 (13)	0.0274 (9)	0.0136 (10)	0.0061 (8)	0.0017 (8)
F3	0.0284 (6)	0.0817 (10)	0.0686 (9)	0.0057 (6)	0.0183 (6)	0.0109 (7)
O3	0.0274 (8)	0.173 (2)	0.0483 (9)	−0.0018 (11)	0.0095 (7)	−0.0078 (12)
N3	0.0466 (10)	0.0540 (11)	0.0359 (9)	−0.0075 (8)	0.0171 (7)	−0.0036 (8)
C3	0.0333 (10)	0.0366 (11)	0.0523 (12)	−0.0003 (8)	0.0016 (8)	−0.0037 (9)
F4	0.0568 (8)	0.0738 (9)	0.0346 (6)	0.0064 (7)	0.0175 (5)	0.0087 (6)
O4	0.0555 (10)	0.148 (2)	0.0449 (9)	−0.0032 (12)	0.0271 (8)	0.0004 (11)
N4	0.0359 (8)	0.0431 (10)	0.0388 (8)	0.0022 (7)	0.0142 (7)	0.0031 (7)
C4	0.0351 (9)	0.0316 (10)	0.0401 (10)	0.0002 (8)	0.0092 (8)	0.0019 (8)
C5	0.0339 (9)	0.0225 (8)	0.0291 (8)	0.0013 (7)	0.0035 (7)	0.0003 (6)
C6	0.0336 (9)	0.0257 (9)	0.0325 (9)	0.0008 (7)	0.0069 (7)	0.0009 (7)
C7	0.0341 (9)	0.0239 (8)	0.0313 (8)	0.0008 (7)	0.0054 (7)	−0.0008 (7)
C8	0.0314 (8)	0.0219 (8)	0.0263 (8)	0.0010 (7)	0.0034 (6)	−0.0001 (6)
C9	0.0265 (8)	0.0333 (9)	0.0340 (9)	0.0006 (7)	0.0073 (7)	−0.0007 (7)

C10	0.0304 (8)	0.0399 (10)	0.0293 (8)	0.0011 (8)	0.0125 (7)	−0.0002 (7)
C11	0.0284 (8)	0.0269 (8)	0.0243 (7)	0.0018 (7)	0.0070 (6)	−0.0010 (6)
C12	0.0262 (8)	0.0274 (8)	0.0274 (8)	0.0010 (7)	0.0079 (6)	0.0005 (6)
C13	0.0315 (8)	0.0271 (8)	0.0258 (8)	0.0002 (7)	0.0102 (6)	−0.0006 (6)
C14	0.0427 (10)	0.0547 (13)	0.0267 (9)	0.0001 (9)	0.0109 (8)	0.0008 (8)
C15	0.0310 (9)	0.0517 (12)	0.0334 (9)	0.0010 (9)	0.0034 (7)	0.0007 (8)
C16	0.0268 (8)	0.0279 (9)	0.0471 (10)	0.0020 (7)	0.0110 (7)	−0.0039 (8)
C17	0.0422 (10)	0.0286 (9)	0.0315 (9)	−0.0002 (8)	0.0077 (7)	−0.0037 (7)
C18	0.0307 (9)	0.0296 (9)	0.0367 (9)	−0.0012 (7)	−0.0023 (7)	0.0005 (7)
C19	0.0231 (8)	0.0405 (11)	0.0453 (10)	0.0005 (7)	0.0078 (7)	0.0066 (8)
C20	0.0351 (9)	0.0379 (10)	0.0313 (9)	0.0007 (8)	0.0080 (7)	0.0054 (7)
C21	0.0264 (8)	0.0230 (8)	0.0368 (9)	−0.0009 (7)	−0.0002 (7)	0.0004 (7)
C22	0.0331 (9)	0.0234 (9)	0.0430 (10)	−0.0008 (7)	−0.0004 (8)	0.0004 (7)
C23	0.0337 (9)	0.0230 (9)	0.0439 (10)	−0.0005 (7)	−0.0007 (8)	0.0005 (7)
C24	0.0301 (8)	0.0204 (8)	0.0352 (9)	−0.0014 (7)	−0.0006 (7)	−0.0010 (7)
C25	0.0271 (8)	0.0279 (9)	0.0414 (10)	−0.0033 (7)	0.0084 (7)	−0.0009 (7)
C26	0.0347 (9)	0.0336 (10)	0.0274 (8)	−0.0049 (8)	0.0076 (7)	−0.0015 (7)
C27	0.0270 (8)	0.0334 (9)	0.0274 (8)	−0.0037 (7)	0.0030 (6)	0.0003 (7)
C28	0.0282 (8)	0.0269 (8)	0.0309 (8)	−0.0008 (7)	0.0075 (6)	−0.0009 (7)
C29	0.0368 (9)	0.0259 (9)	0.0270 (8)	0.0008 (7)	0.0034 (7)	−0.0010 (7)

Geometric parameters (Å, º)

F1—C16	1.340 (2)	C10—H10	0.9500
O1—N3	1.217 (2)	C11—C12	1.403 (2)
N1—C2	1.323 (3)	C12—C13	1.383 (2)
N1—C3	1.337 (3)	C12—H12	0.9500
C1—C2	1.386 (3)	C13—H13	0.9500
C1—C5	1.393 (3)	C14—H14A	0.9800
C1—H1	0.9500	C14—H14B	0.9800
F2—C17	1.344 (2)	C14—H14C	0.9800
O2—N3	1.229 (2)	C15—H15A	0.9800
N2—C11	1.384 (2)	C15—H15B	0.9800
N2—C15	1.432 (2)	C15—H15C	0.9800
N2—C14	1.449 (2)	C16—C17	1.375 (3)
C2—H2	0.9500	C16—C21	1.384 (3)
F3—C19	1.345 (2)	C17—C18	1.367 (3)
O3—N4	1.202 (2)	C18—C19	1.368 (3)
N3—C26	1.467 (2)	C18—H18	0.9500
C3—C4	1.381 (3)	C19—C20	1.377 (3)
C3—H3	0.9500	C20—C21	1.386 (3)
F4—C20	1.340 (2)	C21—C22	1.425 (2)
O4—N4	1.208 (2)	C22—C23	1.193 (3)
N4—C28	1.467 (2)	C23—C24	1.431 (2)
C4—C5	1.387 (3)	C24—C25	1.393 (3)
C4—H4	0.9500	C24—C29	1.399 (3)
C5—C6	1.428 (2)	C25—C26	1.386 (2)
C6—C7	1.195 (2)	C25—H25	0.9500

C7—C8	1.432 (2)	C26—C27	1.374 (2)
C8—C9	1.388 (2)	C27—C28	1.378 (2)
C8—C13	1.402 (2)	C27—H27	0.9500
C9—C10	1.380 (2)	C28—C29	1.381 (2)
C9—H9	0.9500	C29—H29	0.9500
C10—C11	1.400 (2)		

C2—N1—C3	116.71 (17)	N2—C14—H14C	109.5
C2—C1—C5	118.57 (18)	H14A—C14—H14C	109.5
C2—C1—H1	120.7	H14B—C14—H14C	109.5
C5—C1—H1	120.7	N2—C15—H15A	109.5
C11—N2—C15	120.18 (15)	N2—C15—H15B	109.5
C11—N2—C14	120.10 (15)	H15A—C15—H15B	109.5
C15—N2—C14	117.66 (15)	N2—C15—H15C	109.5
N1—C2—C1	124.36 (19)	H15A—C15—H15C	109.5
N1—C2—H2	117.8	H15B—C15—H15C	109.5
C1—C2—H2	117.8	F1—C16—C17	119.21 (17)
O1—N3—O2	123.95 (17)	F1—C16—C21	119.01 (16)
O1—N3—C26	118.36 (17)	C17—C16—C21	121.77 (17)
O2—N3—C26	117.68 (16)	F2—C17—C18	120.07 (17)
N1—C3—C4	123.58 (19)	F2—C17—C16	118.74 (17)
N1—C3—H3	118.2	C18—C17—C16	121.18 (17)
C4—C3—H3	118.2	C17—C18—C19	117.63 (16)
O3—N4—O4	122.72 (18)	C17—C18—H18	121.2
O3—N4—C28	118.72 (16)	C19—C18—H18	121.2
O4—N4—C28	118.56 (17)	F3—C19—C18	119.63 (16)
C3—C4—C5	119.32 (19)	F3—C19—C20	118.46 (18)
C3—C4—H4	120.3	C18—C19—C20	121.91 (17)
C5—C4—H4	120.3	F4—C20—C19	119.49 (17)
C4—C5—C1	117.46 (16)	F4—C20—C21	119.60 (16)
C4—C5—C6	120.69 (17)	C19—C20—C21	120.90 (17)
C1—C5—C6	121.85 (17)	C16—C21—C20	116.60 (15)
C7—C6—C5	176.3 (2)	C16—C21—C22	120.80 (17)
C6—C7—C8	175.3 (2)	C20—C21—C22	122.60 (17)
C9—C8—C13	118.13 (15)	C23—C22—C21	177.2 (2)
C9—C8—C7	119.27 (16)	C22—C23—C24	177.7 (2)
C13—C8—C7	122.60 (16)	C25—C24—C29	119.69 (15)
C10—C9—C8	121.45 (16)	C25—C24—C23	120.88 (17)
C10—C9—H9	119.3	C29—C24—C23	119.43 (17)
C8—C9—H9	119.3	C26—C25—C24	118.57 (17)
C9—C10—C11	120.53 (16)	C26—C25—H25	120.7
C9—C10—H10	119.7	C24—C25—H25	120.7
C11—C10—H10	119.7	C27—C26—C25	123.32 (16)
N2—C11—C10	120.31 (15)	C27—C26—N3	118.22 (16)
N2—C11—C12	121.26 (15)	C25—C26—N3	118.46 (17)
C10—C11—C12	118.42 (15)	C26—C27—C28	116.56 (16)
C13—C12—C11	120.40 (15)	C26—C27—H27	121.7
C13—C12—H12	119.8	C28—C27—H27	121.7

C11—C12—H12	119.8	C27—C28—C29	123.14 (17)
C12—C13—C8	121.03 (15)	C27—C28—N4	118.16 (15)
C12—C13—H13	119.5	C29—C28—N4	118.70 (15)
C8—C13—H13	119.5	C28—C29—C24	118.69 (16)
N2—C14—H14A	109.5	C28—C29—H29	120.7
N2—C14—H14B	109.5	C24—C29—H29	120.7
H14A—C14—H14B	109.5		

Hydrogen-bond geometry (Å, º)

D—H···*A*	*D*—H	H···*A*	*D*···*A*	*D*—H···*A*
C2—H2···F4^{i}	0.95	2.61	3.364 (2)	137
C4—H4···F3^{ii}	0.95	2.41	3.207 (2)	142
C10—H10···F1^{iii}	0.95	2.44	3.193 (2)	136
C14—H14*A*···O1^{iv}	0.98	2.65	3.535 (3)	150
C14—H14*C*···O1^{v}	0.98	2.62	3.334 (3)	130
C18—H18···N1	0.95	2.30	3.245 (2)	173

Symmetry codes: (i) −*x*+1, −*y*+2, −*z*+1; (ii) *x*, −*y*+3/2, *z*+1/2; (iii) −*x*+1, −*y*+2, −*z*+2; (iv) −*x*+1, *y*+1/2, −*z*+3/2; (v) −*x*+1, *y*−1/2, −*z*+3/2.

3-{2-[4-(Dimethylamino)phenyl]ethynyl}pyridine; 1-[2-(3,5-dinitrophenyl)ethynyl]-2,3,5,6-tetrafluorobenzene (2)

Crystal data

$C_{14}H_4F_4N_2O_4 \cdot C_{15}H_{14}N_2$
M_r = 562.47
Orthorhombic, *Pbcn*
a = 13.131 (4) Å
b = 14.423 (4) Å
c = 26.523 (7) Å
V = 5023 (2) Å^3
Z = 8
F(000) = 2304
D_x = 1.488 Mg m^{-3}
Mo *Kα* radiation, *λ* = 0.71073 Å
Cell parameters from 6048 reflections
θ = 2.2–24.9°
μ = 0.12 mm^{-1}
T = 100 K
Cut block, red
0.30 × 0.20 × 0.15 mm

Data collection

Bruker APEXI CCD diffractometer
Radiation source: fine-focus sealed tube
Graphite monochromator
Detector resolution: 8.3660 pixels mm^{-1}
phi and *ω* scans
Absorption correction: multi-scan (SADABS; Bruker, 2014)
T_{min} = 0.598, T_{max} = 0.746
60342 measured reflections
5554 independent reflections
3976 reflections with $I > 2\sigma(I)$
R_{int} = 0.077
θ_{max} = 27.1°, θ_{min} = 2.1°
h = −16→16
k = −18→18
l = −33→33

Refinement

Refinement on F^2
Least-squares matrix: full
$R[F^2 > 2\sigma(F^2)]$ = 0.056
$wR(F^2)$ = 0.154
S = 1.03
5554 reflections
372 parameters
0 restraints
Primary atom site location: dual
Hydrogen site location: inferred from neighbouring sites
H-atom parameters constrained
$w = 1/[\sigma^2(F_o^2) + (0.0771P)^2 + 2.8101P]$ where $P = (F_o^2 + 2F_c^2)/3$

$(\Delta/\sigma)_{max} < 0.001$
$\Delta\rho_{max} = 0.34$ e Å^{-3}
$\Delta\rho_{min} = -0.27$ e Å^{-3}

Special details

Geometry. All esds (except the esd in the dihedral angle between two l.s. planes) are estimated using the full covariance matrix. The cell esds are taken into account individually in the estimation of esds in distances, angles and torsion angles; correlations between esds in cell parameters are only used when they are defined by crystal symmetry. An approximate (isotropic) treatment of cell esds is used for estimating esds involving l.s. planes.

Fractional atomic coordinates and isotropic or equivalent isotropic displacement parameters (Å^2)

	x	*y*	*z*	U_{iso}*/U_{eq}
F1	0.38474 (11)	0.41632 (9)	0.43737 (5)	0.0380 (4)
O1	0.31801 (13)	0.97332 (11)	0.54808 (6)	0.0346 (4)
N1	0.39262 (14)	0.40849 (12)	0.60892 (7)	0.0277 (4)
C1	0.40199 (16)	0.35428 (14)	0.56857 (8)	0.0249 (4)
H1	0.404321	0.383090	0.536381	0.030*
F2	0.40359 (11)	0.36309 (8)	0.34049 (5)	0.0370 (3)
O2	0.34149 (13)	0.98327 (10)	0.62884 (6)	0.0332 (4)
N2	0.37851 (17)	−0.01111 (13)	0.29567 (7)	0.0367 (5)
C2	0.39061 (16)	0.36700 (15)	0.65390 (9)	0.0282 (5)
H2	0.384300	0.404670	0.683118	0.034*
F3	0.35870 (10)	0.67142 (9)	0.28711 (5)	0.0351 (3)
O3	0.36752 (18)	0.70936 (13)	0.72859 (7)	0.0568 (6)
N3	0.33430 (14)	0.93901 (12)	0.58941 (7)	0.0259 (4)
C3	0.39728 (17)	0.27162 (16)	0.66019 (9)	0.0296 (5)
H3	0.396045	0.245202	0.692996	0.036*
F4	0.33985 (10)	0.72583 (8)	0.38375 (5)	0.0312 (3)
O4	0.37845 (15)	0.57505 (11)	0.69379 (6)	0.0419 (5)
N4	0.37037 (15)	0.65946 (13)	0.69135 (7)	0.0300 (4)
C4	0.40574 (16)	0.21554 (15)	0.61807 (9)	0.0279 (5)
H4	0.409481	0.150057	0.621452	0.034*
C5	0.40866 (16)	0.25686 (14)	0.57060 (8)	0.0245 (4)
C6	0.41423 (16)	0.20425 (14)	0.52504 (9)	0.0266 (5)
C7	0.41224 (16)	0.16104 (14)	0.48619 (9)	0.0266 (5)
C8	0.40680 (15)	0.11544 (14)	0.43836 (8)	0.0247 (4)
C9	0.40617 (16)	0.01862 (14)	0.43342 (8)	0.0256 (5)
H9	0.412462	−0.019045	0.462633	0.031*
C10	0.39657 (16)	−0.02264 (14)	0.38683 (8)	0.0265 (5)
H10	0.395229	−0.088382	0.384679	0.032*
C11	0.38867 (16)	0.03017 (15)	0.34216 (8)	0.0253 (5)
C12	0.39060 (16)	0.12726 (15)	0.34730 (9)	0.0275 (5)
H12	0.385972	0.165304	0.318150	0.033*
C13	0.39914 (16)	0.16776 (14)	0.39422 (8)	0.0269 (5)
H13	0.399829	0.233486	0.396587	0.032*
C14	0.3687 (2)	−0.11100 (16)	0.29177 (9)	0.0383 (6)
H14A	0.308064	−0.131321	0.310226	0.057*
H14B	0.429238	−0.140616	0.306219	0.057*
H14C	0.362319	−0.128576	0.256217	0.057*

C15	0.3625 (2)	0.04253 (18)	0.25039 (9)	0.0384 (6)
H15A	0.416917	0.088593	0.246992	0.058*
H15B	0.296569	0.074181	0.252385	0.058*
H15C	0.363092	0.001212	0.221055	0.058*
C16	0.37692 (17)	0.48011 (15)	0.40039 (8)	0.0257 (5)
C17	0.38694 (17)	0.45312 (14)	0.35105 (8)	0.0259 (5)
C18	0.38115 (16)	0.51602 (15)	0.31196 (8)	0.0260 (5)
H18	0.388326	0.496944	0.277863	0.031*
C19	0.36461 (16)	0.60723 (14)	0.32426 (8)	0.0247 (5)
C20	0.35458 (15)	0.63559 (14)	0.37361 (8)	0.0243 (4)
C21	0.36105 (15)	0.57272 (15)	0.41342 (8)	0.0230 (4)
C22	0.35608 (16)	0.60451 (15)	0.46421 (8)	0.0246 (5)
C23	0.35522 (15)	0.63854 (14)	0.50532 (8)	0.0241 (4)
C24	0.35445 (15)	0.68955 (14)	0.55165 (8)	0.0230 (4)
C25	0.34476 (15)	0.78594 (14)	0.54866 (8)	0.0222 (4)
H25	0.337937	0.815635	0.516863	0.027*
C26	0.34526 (15)	0.83733 (14)	0.59255 (8)	0.0219 (4)
C27	0.35444 (15)	0.79785 (14)	0.63971 (8)	0.0227 (4)
H27	0.354911	0.834366	0.669514	0.027*
C28	0.36292 (16)	0.70242 (14)	0.64131 (8)	0.0230 (4)
C29	0.36315 (15)	0.64641 (15)	0.59890 (8)	0.0237 (4)
H29	0.368998	0.580953	0.601686	0.028*

Atomic displacement parameters (Å²)

	U^{11}	U^{22}	U^{33}	U^{12}	U^{13}	U^{23}
F1	0.0628 (9)	0.0243 (7)	0.0268 (7)	0.0032 (6)	−0.0021 (6)	0.0041 (5)
O1	0.0487 (10)	0.0253 (8)	0.0298 (9)	0.0004 (7)	0.0012 (7)	0.0056 (7)
N1	0.0263 (10)	0.0220 (9)	0.0347 (11)	−0.0017 (7)	−0.0006 (8)	−0.0041 (8)
C1	0.0241 (10)	0.0233 (10)	0.0272 (11)	−0.0025 (8)	0.0012 (9)	0.0003 (9)
F2	0.0609 (9)	0.0185 (6)	0.0316 (7)	0.0055 (6)	−0.0031 (6)	−0.0035 (5)
O2	0.0483 (10)	0.0183 (7)	0.0331 (9)	−0.0033 (7)	−0.0010 (7)	−0.0034 (7)
N2	0.0605 (14)	0.0261 (10)	0.0234 (10)	0.0054 (9)	0.0015 (9)	−0.0002 (8)
C2	0.0262 (11)	0.0269 (11)	0.0315 (12)	−0.0023 (9)	−0.0021 (9)	−0.0045 (9)
F3	0.0536 (9)	0.0235 (7)	0.0284 (7)	0.0001 (6)	−0.0021 (6)	0.0048 (5)
O3	0.1175 (19)	0.0299 (9)	0.0229 (9)	0.0151 (10)	−0.0008 (10)	−0.0027 (7)
N3	0.0301 (10)	0.0204 (9)	0.0272 (10)	−0.0038 (7)	0.0008 (8)	0.0010 (8)
C3	0.0274 (11)	0.0332 (12)	0.0283 (12)	−0.0010 (9)	−0.0011 (9)	0.0027 (9)
F4	0.0406 (8)	0.0183 (6)	0.0347 (7)	0.0013 (5)	0.0000 (6)	−0.0034 (5)
O4	0.0763 (13)	0.0191 (8)	0.0304 (9)	0.0048 (8)	−0.0007 (9)	0.0040 (7)
N4	0.0433 (12)	0.0224 (9)	0.0242 (10)	0.0052 (8)	0.0021 (8)	0.0009 (8)
C4	0.0252 (11)	0.0214 (10)	0.0372 (13)	0.0007 (8)	−0.0004 (9)	0.0000 (9)
C5	0.0195 (10)	0.0237 (10)	0.0303 (12)	−0.0010 (8)	−0.0005 (9)	−0.0043 (9)
C6	0.0234 (11)	0.0213 (10)	0.0353 (13)	−0.0011 (8)	0.0000 (9)	−0.0012 (9)
C7	0.0219 (11)	0.0215 (10)	0.0363 (13)	−0.0017 (8)	0.0005 (9)	−0.0002 (9)
C8	0.0213 (10)	0.0221 (10)	0.0307 (12)	0.0003 (8)	0.0021 (9)	−0.0025 (9)
C9	0.0287 (11)	0.0227 (10)	0.0254 (11)	0.0014 (9)	0.0029 (9)	0.0030 (9)
C10	0.0327 (12)	0.0179 (10)	0.0289 (12)	0.0032 (9)	0.0024 (9)	0.0020 (9)

C11	0.0257 (11)	0.0257 (11)	0.0245 (11)	0.0025 (8)	0.0045 (9)	−0.0004 (9)
C12	0.0284 (11)	0.0225 (10)	0.0314 (12)	−0.0002 (9)	−0.0005 (9)	0.0067 (9)
C13	0.0259 (11)	0.0174 (10)	0.0373 (13)	−0.0013 (8)	−0.0003 (9)	0.0007 (9)
C14	0.0584 (17)	0.0290 (12)	0.0274 (12)	0.0103 (11)	−0.0044 (11)	−0.0066 (10)
C15	0.0481 (15)	0.0419 (14)	0.0253 (12)	0.0069 (11)	0.0016 (11)	0.0038 (11)
C16	0.0314 (11)	0.0224 (10)	0.0233 (11)	−0.0005 (9)	−0.0023 (9)	0.0030 (9)
C17	0.0311 (12)	0.0178 (10)	0.0288 (12)	0.0020 (8)	−0.0024 (9)	−0.0025 (9)
C18	0.0320 (12)	0.0252 (11)	0.0209 (10)	−0.0020 (9)	−0.0017 (9)	−0.0033 (9)
C19	0.0272 (11)	0.0218 (10)	0.0251 (11)	−0.0009 (8)	−0.0032 (9)	0.0032 (9)
C20	0.0239 (11)	0.0193 (10)	0.0299 (11)	−0.0007 (8)	−0.0008 (9)	−0.0032 (9)
C21	0.0209 (10)	0.0254 (11)	0.0226 (11)	−0.0006 (8)	−0.0021 (8)	−0.0023 (8)
C22	0.0235 (11)	0.0246 (10)	0.0258 (12)	−0.0007 (8)	0.0003 (8)	−0.0001 (9)
C23	0.0224 (10)	0.0237 (10)	0.0263 (11)	−0.0010 (8)	0.0016 (8)	0.0016 (9)
C24	0.0217 (10)	0.0247 (10)	0.0227 (11)	−0.0005 (8)	0.0017 (8)	−0.0024 (8)
C25	0.0200 (10)	0.0254 (10)	0.0213 (10)	−0.0017 (8)	0.0006 (8)	0.0019 (8)
C26	0.0204 (10)	0.0188 (10)	0.0264 (11)	−0.0025 (8)	0.0020 (8)	0.0005 (8)
C27	0.0223 (10)	0.0229 (10)	0.0229 (11)	−0.0008 (8)	0.0014 (8)	−0.0027 (8)
C28	0.0264 (10)	0.0216 (10)	0.0212 (11)	0.0007 (8)	0.0020 (8)	0.0009 (8)
C29	0.0246 (10)	0.0207 (10)	0.0258 (11)	0.0013 (8)	0.0014 (8)	−0.0024 (8)

Geometric parameters (Å, º)

F1—C16	1.349 (2)	C10—H10	0.9500
O1—N3	1.222 (2)	C11—C12	1.407 (3)
N1—C1	1.331 (3)	C12—C13	1.379 (3)
N1—C2	1.335 (3)	C12—H12	0.9500
C1—C5	1.409 (3)	C13—H13	0.9500
C1—H1	0.9500	C14—H14A	0.9800
F2—C17	1.346 (2)	C14—H14B	0.9800
O2—N3	1.229 (2)	C14—H14C	0.9800
N2—C11	1.376 (3)	C15—H15A	0.9800
N2—C15	1.444 (3)	C15—H15B	0.9800
N2—C14	1.450 (3)	C15—H15C	0.9800
C2—C3	1.388 (3)	C16—C17	1.372 (3)
C2—H2	0.9500	C16—C21	1.395 (3)
F3—C19	1.354 (2)	C17—C18	1.380 (3)
O3—N4	1.223 (2)	C18—C19	1.373 (3)
N3—C26	1.476 (3)	C18—H18	0.9500
C3—C4	1.384 (3)	C19—C20	1.378 (3)
C3—H3	0.9500	C20—C21	1.394 (3)
F4—C20	1.343 (2)	C21—C22	1.424 (3)
O4—N4	1.224 (2)	C22—C23	1.196 (3)
N4—C28	1.468 (3)	C23—C24	1.432 (3)
C4—C5	1.393 (3)	C24—C25	1.398 (3)
C4—H4	0.9500	C24—C29	1.404 (3)
C5—C6	1.429 (3)	C25—C26	1.380 (3)
C6—C7	1.204 (3)	C25—H25	0.9500
C7—C8	1.431 (3)	C26—C27	1.380 (3)

C8—C13	1.396 (3)	C27—C28	1.381 (3)
C8—C9	1.403 (3)	C27—H27	0.9500
C9—C10	1.377 (3)	C28—C29	1.385 (3)
C9—H9	0.9500	C29—H29	0.9500
C10—C11	1.412 (3)		

C1—N1—C2	117.19 (19)	N2—C14—H14C	109.5
N1—C1—C5	124.1 (2)	H14A—C14—H14C	109.5
N1—C1—H1	117.9	H14B—C14—H14C	109.5
C5—C1—H1	117.9	N2—C15—H15A	109.5
C11—N2—C15	121.85 (19)	N2—C15—H15B	109.5
C11—N2—C14	120.17 (19)	H15A—C15—H15B	109.5
C15—N2—C14	117.4 (2)	N2—C15—H15C	109.5
N1—C2—C3	123.4 (2)	H15A—C15—H15C	109.5
N1—C2—H2	118.3	H15B—C15—H15C	109.5
C3—C2—H2	118.3	F1—C16—C17	119.53 (19)
O1—N3—O2	124.52 (18)	F1—C16—C21	118.96 (19)
O1—N3—C26	118.06 (17)	C17—C16—C21	121.49 (19)
O2—N3—C26	117.42 (17)	F2—C17—C16	119.19 (19)
C4—C3—C2	119.2 (2)	F2—C17—C18	119.14 (19)
C4—C3—H3	120.4	C16—C17—C18	121.7 (2)
C2—C3—H3	120.4	C19—C18—C17	117.4 (2)
O3—N4—O4	123.07 (19)	C19—C18—H18	121.3
O3—N4—C28	118.66 (18)	C17—C18—H18	121.3
O4—N4—C28	118.26 (18)	F3—C19—C18	119.44 (19)
C3—C4—C5	118.8 (2)	F3—C19—C20	118.86 (18)
C3—C4—H4	120.6	C18—C19—C20	121.7 (2)
C5—C4—H4	120.6	F4—C20—C19	119.46 (19)
C4—C5—C1	117.34 (19)	F4—C20—C21	119.16 (19)
C4—C5—C6	122.59 (19)	C19—C20—C21	121.37 (19)
C1—C5—C6	120.0 (2)	C20—C21—C16	116.36 (19)
C7—C6—C5	175.7 (2)	C20—C21—C22	120.27 (19)
C6—C7—C8	175.9 (2)	C16—C21—C22	123.3 (2)
C13—C8—C9	117.3 (2)	C23—C22—C21	174.2 (2)
C13—C8—C7	119.91 (19)	C22—C23—C24	173.3 (2)
C9—C8—C7	122.7 (2)	C25—C24—C29	119.92 (19)
C10—C9—C8	121.0 (2)	C25—C24—C23	117.56 (19)
C10—C9—H9	119.5	C29—C24—C23	122.52 (19)
C8—C9—H9	119.5	C26—C25—C24	119.05 (19)
C9—C10—C11	121.75 (19)	C26—C25—H25	120.5
C9—C10—H10	119.1	C24—C25—H25	120.5
C11—C10—H10	119.1	C27—C26—C25	122.92 (19)
N2—C11—C12	121.3 (2)	C27—C26—N3	118.03 (18)
N2—C11—C10	121.70 (19)	C25—C26—N3	119.05 (19)
C12—C11—C10	117.0 (2)	C26—C27—C28	116.51 (19)
C13—C12—C11	120.7 (2)	C26—C27—H27	121.7
C13—C12—H12	119.7	C28—C27—H27	121.7
C11—C12—H12	119.7	C27—C28—C29	123.8 (2)

C12—C13—C8	122.23 (19)	C27—C28—N4	116.99 (18)
C12—C13—H13	118.9	C29—C28—N4	119.20 (18)
C8—C13—H13	118.9	C28—C29—C24	117.79 (19)
N2—C14—H14A	109.5	C28—C29—H29	121.1
N2—C14—H14B	109.5	C24—C29—H29	121.1
H14A—C14—H14B	109.5		

Hydrogen-bond geometry (Å, º)

D—H···*A*	*D*—H	H···*A*	*D*···*A*	*D*—H···*A*
C29—H29···N1	0.95	2.51	3.463 (3)	178
C2—H2···O4	0.95	2.47	3.186 (3)	132
C15—H15*C*···O2^{i}	0.98	2.47	3.257 (3)	137
C18—H18···O4^{i}	0.95	2.46	3.398 (3)	168

Symmetry code: (i) x, $-y+1$, $z-1/2$.